Phase field modeling of brittle fracture in an Euler-Bernoulli beam accounting for transverse part-through cracks

Wenyu Lai[a], Jian Gao[a], Yihuan Li[a], Marino Arroyo[b], Yongxing Shen[a,*]

[a] *University of Michigan – Shanghai Jiao Tong University Joint Institute, Shanghai Jiao Tong University, Shanghai, China*

[b] *Laboratori de Càlcul Numèric, Universitat Politècnica de Catalunya (UPC BarcelonaTech), Barcelona, Spain*

Abstract

We present a phase field model to simulate brittle fracture in an initially straight Euler-Bernoulli beam, with generalization to curved beams. We start from formulating the problem with the principle of minimum potential energy in a 3D solid, with the displacement field and the phase field as primary arguments. We then select, for each cross section, representative fields that characterize the said cross section, including the beam deflection and rotation, and two independent ansatz variables within the cross section to represent the phase field. The problem then reduces to a minimization with only one-dimensional field variables. A feature of the proposed method is, without discretizing the phase field within the cross section, it can represent its variation within the cross section, allowing to simulate cracks partially going through the thickness due to bending as well as axial loads.

Keywords: Phase field, Euler-Bernoulli beam, Brittle fracture, Dimension reduction

1. Introduction

The study of fracture behavior of a slender column or beam with cracks is a problem of practical interest and of crucial importance to aerospace,

*800 Dongchuan Road, University of Michigan – Shanghai Jiao Tong University Joint Institute, Shanghai Jiao Tong University, Shanghai, 200240, China

Email address: yongxing.shen@sjtu.edu.cn (Yongxing Shen)

mechanical and civil engineering. According to Irwin and Paris [1], the stress near crack tips is concentrated and thus induces a local reduction in the stiffness of the structure member which, in turn, alters the static and dynamic behaviors of the structure. Following this idea, Okamura *et al.* [2] proposed the local flexibility approach, in which the local flexibility due to an edge crack is modeled by a massless rotational spring connecting two pristine parts. The stiffness of the rotational spring is expressed in terms of stress intensity factors derived from linear elastic fracture mechanics.

Christides and Barr [3] modified the Euler-Bernoulli beam theory to include the effect of one or more pairs of symmetric open cracks in a structural member of simple geometric form. In Bouboulas *et al.* [4], a cracked beam finite element for the modeling of fractured skeletal structures is introduced. The stiffness matrix of the cracked beam element is derived by using the direct stiffness method, which is a function of the crack depth and position. Vo-Duy *et al.* [5] modeled the damage by the reduction of longitudinal and transverse Young's moduli of a specific beam layer of a laminated composite beam structure.

As beam and shell formulations are both dimension-reduction ones, below we review some of the recent works on shell fractures. Areias and Belytschko [6] developed an extended finite element procedure for analyzing arbitrary crack propagation in shells. Areias *et al.* [7] then made significant improvements to the aforementioned method. Nevertheless, in both contributions, the cracks are assumed to be through the thickness.

The phase field approach is an alternative method to model crack initiation, propagation, and branching without any *ad hoc* criteria or the need to track the complex geometry. This approach was proposed by Bourdin *et al.* [8] based on the variational formulation of brittle fracture by Francfort and Marigo [9]. The main idea is using a diffusive auxiliary scalar field, called the phase field, to represent intermediate states between the fully broken and intact material states. The phase field, along with displacement field, is determined from a minimization principle in the static case. For a more detailed review of the phase field method, see Ambati *et al.* [10].

Due to the advantages mentioned above, a few researchers have applied the phase field method to plate and shell fracture. Modeling the shell as an assembly of flat finite elements, Ulmer *et al.* [11] decompose the strain tensor into membrane and bending parts, and then also split the strain energy accordingly. Amiri *et al.* [12] presented a phase field model for fracture in thin shells, which possesses a number of distinct features. First, the shell

geometry is represented by a scattered point sets based on statistical learning techniques. Second, both the displacement field and the phase field are interpolated with the local maximum-entropy meshfree method. However, in [12], the phase field is assumed constant within the thickness of the shell, precluding the representation of progressive damaging of the shell sections in bending-dominated cases.

A more recent contribution to this issue is addressed by Areias *et al.* [13]. To recover a physically meaningful behavior in bending, they introduced two independent phase fields to identify damage at the upper and lower faces of a shell, respectively. In the discretization step, these two phase fields are interpolated separately within their own surface, while between the upper and lower surfaces, linear interpolation is adopted.

Ambati *et al.* [14] applied the phase field approach to model fracture in a solid-shell with tension-compression split according to either [15] or [16]. Kiendl *et al.* [17] proposed a new approach, where both tension term and compression term depend on the total strain consisting of membrane and bending deformation. In contrast to previous developments, Reinoso *et al.* [18] presented a phase field model for large deformation analysis of thin-walled structures using an enhanced strain-based formulation, coupling with the displacement and the incompatible strain fields.

In this paper, we develop a one-dimensional formulation for modeling the brittle fracture in an Euler-Bernoulli beam under bending load, with the aim of generalizing it to plate and shell problems. This formulation is one-dimensional in the sense that all primary variables are functions of only x, the coordinate along the beam axis. Moreover, we restrict the cracks to be perpendicular to the beam axis, and also the deformation to be plane strain in a plane that contains the beam axis.

With such restrictions, this model is capable of taking into account cracks emanating from the edge and extending only a fraction of the beam height, such as those caused by bending load. This is accomplished by a non-constant phase field across the thickness. More precisely, we introduce a specially designed phase field ansatz, a double-sigmoid function, to represent the phase field variation across the thickness. The ansatz expression only as two parameters to be determined, themselves being functions of x. The idea to adopt a double-sigmoid form is twofold. First, their limiting behavior as the transition widths of the sigmoids vanish resembles piecewise constant functions with desired values of 0 and 1. Second, this transition width at finite values can be tied to the length-scale parameter of the phase field method in

the bulk form.

The ability to handle part-through cracks seems contradictory to the assumptions of small cross section induced in the Euler-Bernoulli theory. In fact, the purpose of doing so is to test the double-sigmoid ansatz in the simplest setting; the formulation is applicable to any displacement assumptions such as the Timoshenko beam theory, and with appropriate generalizations, also to shell fracture problems.

The structure of the remainder of the paper is as follows: Section 2 recapitulates the bulk formulation of phase field models for brittle fracture. Section 3 specializes the formulation to the Euler-Bernouli beam, including the ansatz for the phase field. In Section 4 implementation details of the method are provided, while in Section 5 numerical examples with straight and curved beams that showcase the capability of the proposed model are given, including a comparison with bulk computation. Finally, in Section 6, conclusions are drawn concerning the results of the proposed approach.

2. Recapitulation of a phase field model for brittle fracture

This section recapitulates a phase field model for brittle fracture in the quasi-static setting. The reader is referred to [19, 9, 8] for more variations and analysis of similar models.

Consider a bounded Lipschitz continuous domain $\Omega \subset \mathbb{R}^n$, $n = 2$ or 3. The boundary of this domain, $\partial\Omega$, is divided into Dirichlet boundary Γ_D and Neumann boundary Γ_N such that $\Gamma_D \cup \Gamma_N = \partial\Omega$ and $\Gamma_D \cap \Gamma_N = \emptyset$. In the quasi-static case, the model is based on minimizing the system's total potential energy functional of $\boldsymbol{u} \in H^1(\Omega, \mathbb{R}^n)$, the displacement field, and $d \in H^1(\Omega)$, the phase field. This energy functional takes the following form:

$$\begin{aligned}\Pi[\boldsymbol{u}, d] := \int_\Omega \psi[\boldsymbol{\varepsilon}(\boldsymbol{u}), d]\, d\Omega - \int_{\Gamma_N} \boldsymbol{t}_N \cdot \boldsymbol{u}\, d\Gamma - \int_\Omega \boldsymbol{b} \cdot \boldsymbol{u}\, d\Omega \\ + g_c \int_\Omega \gamma(d, \nabla d)\, d\Omega,\end{aligned} \tag{1}$$

where the *surface density function* per unit volume of the solid is introduced as

$$\gamma(d, \nabla d) = \frac{d^2}{2\ell} + \frac{\ell}{2}|\nabla d|^2. \tag{2}$$

Note that in the work of [8], for example, the phase field v is defined as $1 - d$ in our notation. Here vector fields $\boldsymbol{u}_D : \Gamma_D \to \mathbb{R}^n$, $\boldsymbol{t}_N : \Gamma_N \to \mathbb{R}^n$,

and $\boldsymbol{b} : \Omega \to \mathbb{R}^n$ are prescribed displacement, traction, and body force fields, respectively. Scalars g_c and ℓ are the critical energy release rate and the phase field length scale parameter, respectively. Tensor $\boldsymbol{\varepsilon}$ is the strain defined as

$$\boldsymbol{\varepsilon}(\boldsymbol{u}) := \frac{1}{2}\left(\nabla \boldsymbol{u} + (\nabla \boldsymbol{u})^T\right).$$

In this work, we consider a strain energy density $\psi[\boldsymbol{\varepsilon}(\boldsymbol{u}), d]$ that takes the following form:

$$\psi(\boldsymbol{\varepsilon}, d) = (1-d)^2 \psi_+(\boldsymbol{\varepsilon}) + \psi_-(\boldsymbol{\varepsilon}). \tag{3}$$

Scalar functions ψ_+ and ψ_- are the strain energy densities due to tension and compression, respectively, which must satisfy

1. $\psi_+(\boldsymbol{\varepsilon}), \psi_-(\boldsymbol{\varepsilon}) \geq 0$ for all $\boldsymbol{\varepsilon}$;
2. $\psi_+(\boldsymbol{\varepsilon}) + \psi_-(\boldsymbol{\varepsilon}) = \psi_0(\boldsymbol{\varepsilon})$, where ψ_0 is the strain energy density function of a pristine elastic solid. For a linear isotropic model, ψ_0 is given by

$$\psi_0(\boldsymbol{\varepsilon}) = \frac{\lambda}{2}(\operatorname{tr} \boldsymbol{\varepsilon})^2 + \mu \boldsymbol{\varepsilon} : \boldsymbol{\varepsilon},$$

where λ and μ are Lamé constants which satisfy $\mu > 0$ and $\lambda + 2\mu > 0$.

From (3), the stress-strain relation is given by

$$\boldsymbol{\sigma}(\boldsymbol{\varepsilon}, d) = \frac{\partial \psi(\boldsymbol{\varepsilon}, d)}{\partial \boldsymbol{\varepsilon}} = (1-d)^2 \boldsymbol{\sigma}_+(\boldsymbol{\varepsilon}) + \boldsymbol{\sigma}_-(\boldsymbol{\varepsilon}), \tag{4a}$$

where $\boldsymbol{\sigma}_\pm(\boldsymbol{\varepsilon}) := \partial \psi_\pm(\boldsymbol{\varepsilon}) / \partial \boldsymbol{\varepsilon}$.

The choice of $\psi_+(\boldsymbol{\varepsilon})$, and thus $\psi_-(\boldsymbol{\varepsilon})$, is not unique in the literature. Earlier works such as [8, 20, 21, 22] essentially set $\psi_+(\boldsymbol{\varepsilon}) = \psi_0(\boldsymbol{\varepsilon})$, leading to an analytic expression of $\psi(\boldsymbol{\varepsilon}, d)$. Nevertheless, this model treats tension and compression alike, resulting in unphysical crack propagation due to compression.

In contrast, Amor *et al.* [15] and Miehe *et al.* [16] proposed models that split the contribution to the internal energy from tension (or dilatation) and compression. In this work, we will adopt the model proposed in [16], which reads

$$\psi_+(\boldsymbol{\varepsilon}) = \frac{\lambda}{2}\langle \operatorname{tr} \boldsymbol{\varepsilon} \rangle_+^2 + \mu \sum_{i=1}^{3} \langle \varepsilon_i \rangle_+^2, \tag{4b}$$

where ε_i, $i = 1, 2, 3$, are principal strains, and $\langle x \rangle_+ := (x + |x|)/2$ is the McCaulay bracket.

3. Specialization to an Euler-Bernoulli beam

In this section, we specialize the phase field formulation (1) to the case in which Ω takes the geometry of a prismatic beam. We set the origin of an orthonormal basis $(\boldsymbol{e}_x, \boldsymbol{e}_y, \boldsymbol{e}_z)$ to the centroid of one of the basal planes of the beam, with $\boldsymbol{e}_x$ along the beam axis. Let $\Omega = A \times (0, L)$, where L is the length of the beam and the open set $A \subset \mathbb{R}^2$ is the cross section in the yz-plane.

To focus on the main idea, we make the problem essentially two-dimensional in the xy-plane by further assuming that A, and thus Ω, is symmetric about the plane $z = 0$, and that all transverse loads are applied within the xy-plane, see Figure 1.

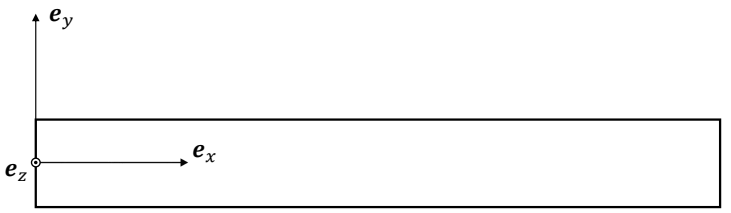

Figure 1: Orthonormal basis for a beam. In this work, we assume that the beam is symmetric about the xy-plane, and that all transverse loads are applied in this plane. These render the problem two-dimensional in the xy-plane.

The goal of this section is to render the formulation essentially one-dimensional, i.e., all primary variables depending only on x. To attain this, we restrict all cracks to be *perpendicular to* $\boldsymbol{e}_x$.

3.1. Kinematics for an initially straight beam

We adopt the Euler-Bernoulli beam theory here for simplicity~~, but the proposed phase field formulation can easily be generalized to the Timoshenko beam theory, for example~~. This theory assumes that the cross section A: (1) is rigid in its own plane, the yz-plane, (2) remains plane after deformation, and (3) is normal to the deformed axis of the beam.

The Euler-Bernoulli assumptions lead to the following kinematic ansatz on the displacement field $\boldsymbol{u} : \Omega \to \mathbb{R}^2$:

$$\boldsymbol{u}(x, y, z) = -(y - y_{na})\overline{v}'(x)\boldsymbol{e}_x + \overline{v}(x)\boldsymbol{e}_y, \tag{5}$$

where $y_{na} = y_{na}(x)$ is the y-coordinate of the neutral axis of the cross section $A(x)$, $\overline{v}(x)$ is the sectional displacement, and $\overline{v}' := d\overline{v}(x)/dx$. In the classical Euler-Bernoulli beam theory, when the section is made of an isotropic homogeneous material, $y_{na} \equiv 0$. However, in our case, due to the possible existence of cracks in the cross section, the neutral axis may *not* go through the centroid of A, but needs to be determined from force equilibrium, see Section 3.4 for more details.

From (5), the strain field is given by,

$$\boldsymbol{\varepsilon}(x, y, z) = -(y - y_{na})\kappa(x)\boldsymbol{e}_x \otimes \boldsymbol{e}_x, \tag{6}$$

where

$$\kappa(x) = \overline{v}''(x),$$

is the sectional curvature about axis $\boldsymbol{e}_z$.

3.2. Constitutive response for an initially straight beam

Specializing the constitutive model (4) for the beam model described in Section 3.1, in particular, the strain field (6) and the condition $\lambda = 0$ and $\mu = E/2$[1], leads to

$$\psi_+(\boldsymbol{\varepsilon}) = \frac{E}{2}\langle -\kappa(y - y_{na})\rangle_+^2,$$

and hence the following constitutive response:

$$\psi(x, y, z) = \frac{1}{2}\zeta(d, \kappa, y, y_{na})E\kappa^2(y - y_{na})^2, \tag{7}$$

$$\boldsymbol{\sigma}(x, y, z) = -\zeta(d, \kappa, y, y_{na})E\kappa(y - y_{na})\boldsymbol{e}_x \otimes \boldsymbol{e}_x, \tag{8}$$

where the *sectional degradation factor* $\zeta(d, \kappa, y, y_{na})$ takes the expression as follows,

$$\zeta(d, \kappa, y, y_{na}) = H[(y - y_{na})\kappa] + (1 - d)^2 H[-(y - y_{na})\kappa].$$

Here $H(\cdot)$ is the Heaviside function defined as $H(x) = 1$ if $x > 0$, $H(x) = 0$ if $x < 0$ and $H(x) = 1/2$ if $x = 0$.

[1]This corresponds to the case of a vanishing Poisson's ratio.

3.3. Ansatz for the phase field over the cross section

To obtain a formulation with the primary fields only dependent on the axial variable x, we assume that the phase field d takes a specific functional form within the cross section, i.e., an ansatz as a field on the beam cross section. To be consistent with the two-dimensional assumption, we will also assume that d does not depend on z.

The simplest possible ansatz for the phase field is a constant function over the cross section, i.e., $d(x, y) = d(x)$. Nevertheless, this ansatz can only represent complete fracture over the cross section, but is unable to describe partial fracture, say fracture caused by a bending load.

To overcome this limitation, we propose a *double-sigmoid* ansatz that takes the following form:

$$d(x, y) = 1 - \frac{1}{2} S\left[\xi_L(x, y)\right] + \frac{1}{2} S\left[\xi_U(x, y)\right], \quad H_L \le y \le H_U, \tag{9}$$

where $H_L := \inf_A y$ and $H_U := \sup_A y$. The sigmoid function $S \in C^3(\mathbb{R})$ is such that

$$S(-\xi) = -S(\xi),\ 0 < S'(\xi) \le 1,\ S(\xi) \to \pm 1 \text{ as } \xi \to \pm\infty,\ S'(\xi) = 1 \text{ iff } \xi = 0.$$

These conditions imply that $S(0) = 0$ and $-1 < S(\xi) < 1$ for all $\xi \in \mathbb{R}$. Here

$$\xi_L(x, y) := \frac{2}{\ell}[y - y_L(x)], \quad \xi_U(x, y) := \frac{2}{\ell}[y - y_U(x)].$$

This ansatz is based on the following assumptions:

1. Cracks only emanate perpendicular to the beam axis from the top or bottom of the beam.
2. The phase field d generally assumes extreme values 0 or 1, except over transition regions with a size of order ℓ.
3. The partial derivative $\partial d/\partial y$ evaluated at $y = y_L$ or y_U almost equals $1/\ell$. This is to match the phase field solution in the bulk case, i.e., $d = \exp(|y|/\ell)$, where the y-axis is perpendicular to the crack with $y = 0$ on the crack path.

For concreteness, we have chosen

$$S(\xi) = \tanh \xi$$

in this work. In addition, regularization parameter ℓ is required to satisfy $\ell \leq (H_U - H_L)/4$. An illustration of this ansatz is given in Figure 2. Here y_L and y_U are ansatz variables which, when lying inside the range (H_L, H_U), represent roughly the y-coordinate of the crack front emanating from the bottom and the top, respectively. In principle, y_L and y_U can assume values of all real numbers with the restriction $y_L < y_U$ ($y_L \geq y_U$ means complete breakage of the cross section). However, to render a tangent stiffness matrix with a manageable conditioning, we require $H_L - \beta\ell \leq y_L < y_U \leq H_U + \beta\ell$ where $\beta \approx 1$. The case of $y_L = H_L - \ell$ and $y_U = H_U + \ell$ is plotted in Figure 3, which shows that the resulting phase field is already very close to a constant zero profile, a profile corresponding to the pristine state of the solid.

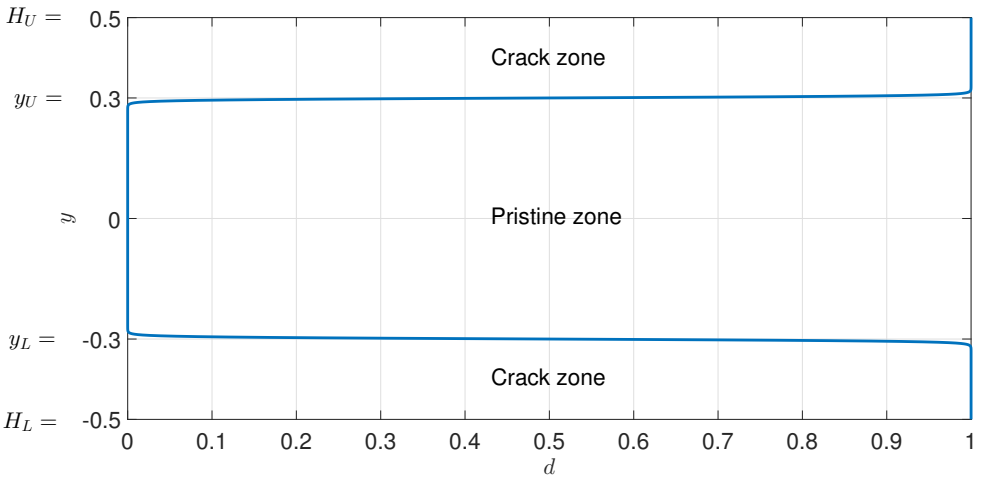

Figure 2: Phase field profile corresponding to a particular choice of ansatz variables $y_L = -0.3, y_U = 0.3$ and $\ell = 0.01$, for a unit beam height $H_U - H_L = 1$. The phase field takes on extreme values except in transition regions near $y = y_L$ and $y = y_U$.

3.4. The neutral axis and the moment of inertia

The location of the neutral axis of any cross section is determined from the axial force equilibrium at that cross section. Since there is no axial load applied,

$$\int_A \sigma_{xx}(x, y, z)\, dydz = 0,$$

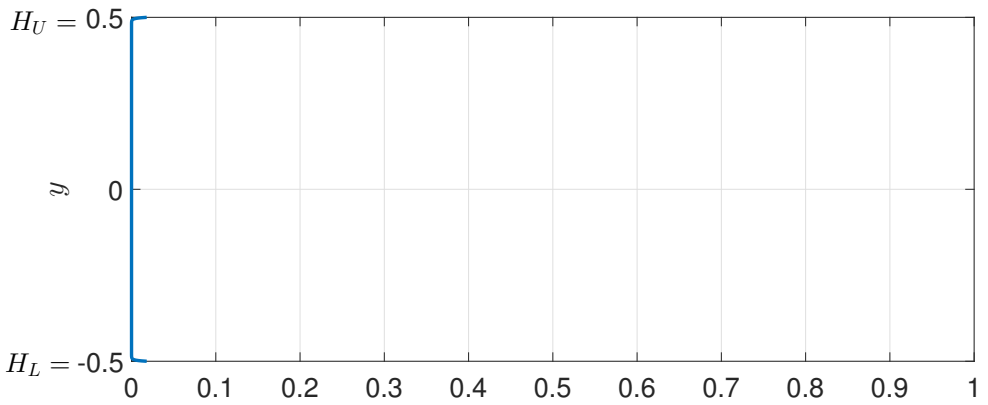

Figure 3: Phase field profile corresponding to extreme values of the ansatz variables $y_L = H_L - \ell$ and $y_U = H_U + \ell$. Here $\ell = 0.01$, for a unit beam height $H_U - H_L = 1$. The resulting phase field is almost constant zero and thus will be regarded as representing the pristine state of the material throughout the cross section.

which reduces to

$$\int_A [y - y_{na}(x)]\ \zeta[d, \kappa(x), y, y_{na}(x)]\ dydz = 0, \tag{10}$$

by virtue of (8). Equation (10) then uniquely determines y_{na} for any x.

From (7), the strain energy density (per unit length) at x takes the form

$$\frac{1}{2} E\kappa(x)^2 \int_A [y - y_{na}(x)]^2\ \zeta[d, \kappa(x), y, y_{na}(x)]\ dydz.$$

As a result, the sectional moment of inertia $I(x)$ is given by

$$I(x) = \int_A \zeta[d, \kappa(x), y, y_{na}(x)]\ [y - y_{na}(x)]^2\ dydz. \tag{11}$$

Sanity check. In the case of a pristine cross section, $d \equiv 0$, then $\zeta(d, \kappa, y, y_{na}) \equiv 1$. In this case, (10) and (11) reduce to their classical form.

3.5. Statement of the problem

Without loss of generality, we consider a cantilever beam occupying $x \in [0, L]$ subjected to essential boundary conditions $\overline{v}(x_V) = v_0$ and $\overline{v}'(x_\theta) = \theta_0$. Moreover, let a concentrated bending moment $M\boldsymbol{e}_z$ be applied at $x_M \in [0, L]$,

a point load $F\boldsymbol{e}_y$ be exerted at point $x_F \in [0, L]$, and distributed load $w\boldsymbol{e}_y$, $w : [0, L] \to \mathbb{R}$, be acting on the entire beam.

Then the total potential functional is given by

$$\begin{aligned}\hat{\Pi}_\ell[\overline{v}, y_L, y_U] &= \Pi_\ell[\overline{v}, d(y_L, y_U)] \\ &= \frac{1}{2}\int_0^L EI(x; \overline{v}, y_L, y_U)\kappa(x)^2\, dx - M\overline{v}'(x_M) - F\overline{v}(x_F) - \int_0^L w(x)\overline{v}(x)dx \\ &\quad + \int_0^L \int_A g_c\gamma[d(x, y; y_L, y_U), \nabla d(x, y; y_L, y_U)]\, dydz\, dx.\end{aligned} \tag{12}$$

We then define

$$\begin{aligned}\mathcal{Y} &= H^1(0, L), \\ \mathcal{V} &= \left\{f \in H^2(0, L) \middle| f(x_V) = v_0, f'(x_\theta) = \theta_0\right\}, \\ \mathcal{V}_0 &= \left\{f \in H^2(0, L) \middle| f(x_V) = 0, f'(x_\theta) = 0\right\}.\end{aligned} \tag{13}$$

Finally, let the initial conditions be

$$y_L(x, t = 0) = y_L^0(x), \quad y_U(x, t = 0) = y_U^0(x). \tag{14}$$

The quasi-static evolution of the coupled problem can be stated as: For a given load history $\{v_0, \theta_0, M, F, w\}$ dependent on a time-like variable $t \in [0, T]$, $T > 0$, and initial conditions (14), find $(\overline{v}, y_L, y_U) \in \mathcal{V} \times \mathcal{Y} \times \mathcal{Y}$, as the minimizer of total potential functional (12), subjected to irreversibility constraints

$$\forall x \in [0, L],\ y_L(x, t_1) \le y_L(x, t_2),\ y_U(x, t_1) \ge y_U(t_2),\ \text{whenever } t_1 < t_2, \tag{15}$$

until either (a) $t = T$ or (b) the early termination criterion $y_L \ge y_U$ is satisfied at some x.

This constrained optimization problem is the basis of the numerical implementation to be detailed in Section 4.

On the strong form. Some of the equations in the strong form, in the simple case of $M = F = 0$ and $x_V = x_\theta = 0$, can be obtained as

$$\begin{aligned}\frac{d^2}{dx^2}[EI(x)\kappa(x)] - w(x) &= 0, \\ \overline{v}(x = 0) = \overline{v}'(x = 0) &= 0, \\ \overline{v}''(x = L) = \overline{v}'''(x = L) &= 0.\end{aligned}$$

The remaining equations are those for the ansatz variables y_L and y_U. Nevertheless, these equations are omitted here as they are too lengthy and tedious to show, although they can be obtained as Karush-Kuhn-Tucker systems using standard procedures of Euler-Lagrange equations.

3.6. Generalization to a curved beam

This section aims to generalize the kinematics of a straight beam to a curved beam. The geometry of the curved beam are characterized by the curvilinear coordinate system (s, r) depicted in Figure 4. Here s and r denote the coordinates along the tangential and thickness directions, respectively. We let $R = R(s)$ represent the radius of curvature at the mid-line of the beam. Angle ϕ is the physical rotation of the section, as shown in Figure 4. Let u and v be the tangential and normal displacements of the neutral axis. Following Gan [23], the displacement field of the curved Euler-Bernoulli beam is given by,

$$\begin{aligned} u(s,r) &= -r\theta(s) - v\frac{d\phi}{ds}, \\ v(s,r) &= v(s), \\ \theta(s) &= \frac{dv}{ds}. \end{aligned}$$

Then, the normal strain field is given by,

$$\varepsilon_s = -r\frac{d\theta}{ds} + \frac{v}{R(s)}.$$

In the simulation, we use the non-uniform rational B-spline (NURBS) to parameterize the curved beam. The other treatments are very similar to the case of a straight beam. In particular, we use R_L and R_U as the phase field ansatz parameters, playing the roles of y_L and y_U, respectively.

4. Numerical implementation

This section details the numerical implementation of the proposed model. In this section, we will first introduce the spatial discretization of the problem in Section 4.1, and then the staggered scheme to solve the coupled problem in Section 4.2.

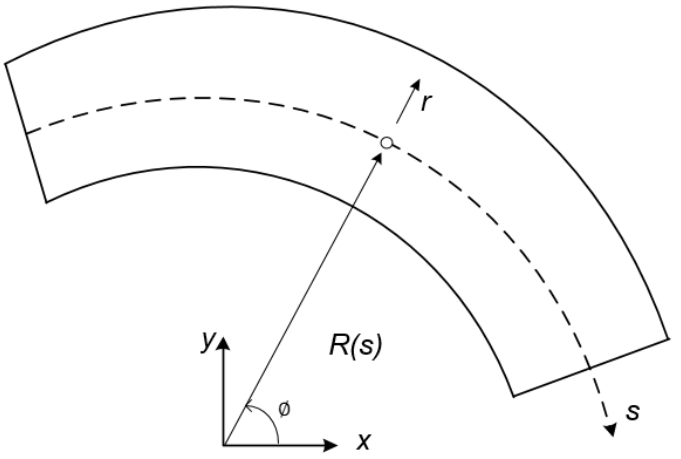

Figure 4: A general curved Euler-Bernoulli beam.

4.1. Finite element discretization of the primary variables

As a reminder, the primary variables of the model are the transverse displacement field $\overline{v}$ and the phase field ansatz variables y_L and y_U, all functions over $[0, L]$. From (13), $\overline{v}$ requires C^1 continuity while y_L and y_U require only C^0. The corresponding lowest order polynomial elements are the Hermit cubic element and the P_1 element, respectively, which are the basis functions we have adopted.

The same quasi-uniform mesh is used for $\overline{v}$, y_L, and y_U, whose largest element length h_e should satisfy $h_e \leq \ell/2$ according to [19]. Usually we prefer the choice with $h_e \leq \ell/4$.

Now let

$$\overline{v}(x) = \sum_{i=1}^{n_v} v_i N_i(x), \quad y_L(x) = \sum_{j=1}^{n_d} y_{Lj}\phi_j(x), \quad y_U(x) = \sum_{j=1}^{n_d} y_{Uj}\phi_j(x), \quad (16)$$

where $N_i \in \mathcal{V}$, $i = 1, \ldots, n_v$, and $\phi_j \in \mathcal{Y}$, $j = 1, \ldots, n_d$. The discrete nonlinear optimization problem to be solved can then be obtained by substituting (16) into (12), subjected to the irresversibility constraints (15) at the nodes, and with the early termination criterion

$$y_{Lj} \geq y_{Uj}, \quad \exists j = 1, \ldots, n_d. \quad (17)$$

Determination of y_{na}. In general, y_{na} has to be determined from (10) iteratively. Note that we always have $\zeta > 0$, implying that the values H_L and H_U always bracket the root of (10). Then any standard root-finding algorithm such as the Pegasus method introduced in [24] is able to obtain the root within a reasonable number of iterations. Alternatively, $y_{na} = y_{na}(x)$ can also be treated as an independent field, whose minimizer of (12) coincides with (10).

Numerical integration along the beam height. The key issue in the implementation is the integration to obtain the residual vector (see Appendix A) and tangent stiffness matrix over the beam height, for each Gauss point for x. A single Gauss integration rule will likely miss the regions with rapidly varying integrands; an adaptive integration rule would be too expensive. Here as we observe that the integrands vary near y_L and y_U. When $y_U - y_L > 4\ell$, we collect critical points $\{y_L \pm 2\ell, y_U \pm 2\ell, y_{na}\}$ and divide the beam height $[-h/2, h/2]$ with such critical points, see Figure 5. Each of the resulting intervals will be integrated using up to four Gauss points.

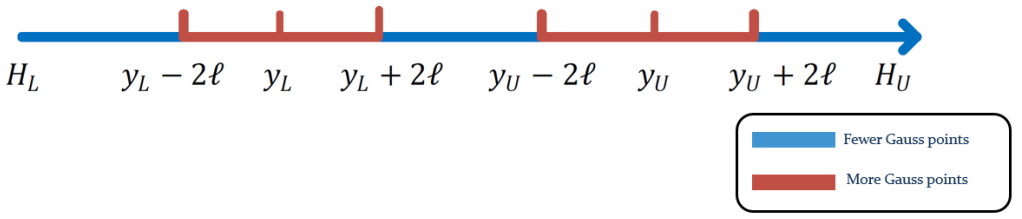

Figure 5: Multi-sections of integration.

4.2. Staggered scheme with the active set method

To begin, we divide the total load history into N_{LS} load steps, i.e., $0 = t_0 < t_1 < \ldots < t_{N_{LS}} = T$ and solve for the solution at each load step t_k, $k = 1, \ldots, N_{LS}$. The entire algorithm is given in Algorithm 1.

For a typical coupled problem, there is usually a decision between a monolithic solution scheme versus a staggered scheme. Here we adopt the latter, which consists of solving two sub-problems alternately until convergence, one for the displacement field and one for the phase field. For the displacement sub-problem, we use the Newton-Raphson method, while for the phase field sub-problem, we use the Newton-Raphson method along with a version of the active set method [25] to enforce the inequality constraints (15).

For each update of y_L and y_U, if (17) is satisfied at any cross section of the beam, the program is terminated, as the corresponding cross section has completely broken.

5. Numerical examples

To better illustrate the proposed methodology, we present several numerical examples. The model material is polymethyl methacrylate, which has a Young's modulus $E = 2.74$ GPa and a critical energy release rate $g_c = 482$ J/m^2 [26]. Note that for the most part of a beam, the initial condition can be set as

$$y_L = H_L - \beta\ell, \quad y_U = H_U + \beta\ell,$$

except for the locations where initial cracks are to be modeled.

5.1. An initially pristine cantilevered beam

We first investigate a pristine cantilevered beam with an upward displacement load imposed at the tip, as depicted in Figure 7.

The displacement load is increased until complete breakage of the cross section near the clamped root. The length parameter $\ell = 20$ mm and $\beta = 1$ is adopted. The numerical experiment is carried out with element sizes $h_e = 20, 10, 5, 2.5$ mm respectively. We expect that for a small enough h_e/ℓ the effect of the mesh size will be insignificant. The comparison of load-deflection curves for different mesh sizes is shown in Figure 8. We can observe that the results are overall mesh independent. The evolution of the phase field, represented by the variation of y_L and y_U, is shown in the left column of Figure 9 where crack initiation and propagation could be observed.

We also compare the 1D beam model with 2D bulk model by using the same material parameters, with Poisson's ratio $\nu = 0$, $\ell = 20$ mm, and mesh size $h_e = 5$ mm. The expression of the strain energy density given by (4b) is adopted. The right column of Figure 9 shows the results under an increasing tip displacement load. The load-displacement curves from the 2D bulk-form phase field method and 1D proposed method are compared in Figure 6. It can be shown that qualitatively these two models behave the same, hence effective stiffness and toughness properties for the 1D model could be derived and modified so as to match the 2D curve, if accurate quantitative analysis is needed.

Algorithm 1: Staggered scheme combined with the active set method

Initialize $\overline{v}$ and $\{y_L, y_U\}$ with initial conditions and set $k = 1$. Define tol_v and tol_d as the tolerances of the normal of residual for displacement and phase field sub-problem, respectively;

Set $0 = t_0 < t_1 < \ldots < t_{N_{LS}} = T$;

Let $\overline{\mathbf{v}}$, $\mathbf{y}_L$, and $\mathbf{y}_U$ denote collections of nodal degrees of freedom of $\overline{v}$, y_L, and y_U, respectively;

while $k \leq N_{LS}$ **do**

  Update the loads $\{v_0, \theta_0, M, F, w\}$ for $t = t_k$;

  repeat

    `/* Fix the phase field and update the displacement field */`

    Compute tangent stiffness matix $\mathbf{K}_v$ and residual $\mathbf{R}_v$ of the displacement sub-problem;

    $\overline{\mathbf{v}} \leftarrow \overline{\mathbf{v}} - \mathbf{K}_v^{-1}\mathbf{R}_v$;

    `/* Fix the displacement field and update the phase field */`

    Set $\mathscr{A}_L = \mathscr{A}_U = \{j \in \mathbb{N} : 1 \leq j \leq n_d\}$;

    repeat

      Set flag $\leftarrow$ false;

      Compute tangent stiffness matix $\mathbf{K}_d$ and residual $\mathbf{R}_d = \{\mathbf{R}_L^T, \mathbf{R}_U^T\}^T$ of the phase field sub-problem;

      Set $\mathscr{A}_L \leftarrow \mathscr{A}_L \cup \{j : R_{Lj} < 0\}$;

      Set $\mathscr{A}_U \leftarrow \mathscr{A}_U \cup \{j : R_{Uj} > 0\}$;

      For all j such that $y_{Lj} < y_{Lj}^{k-1}$, set $\mathscr{A}_L \leftarrow \mathscr{A}_L \setminus \{j\}$ and $y_{Lj} \leftarrow y_{Lj}^{k-1}$;

      For all j such that $y_{Uj} > y_{Uj}^{k-1}$, set $\mathscr{A}_U \leftarrow \mathscr{A}_U \setminus \{j\}$ and $y_{Uj} \leftarrow y_{Uj}^{k-1}$;

      Update $\{y_{Lj} : j \in \mathscr{A}_L\} \cup \{y_{Uj} : j \in \mathscr{A}_U\}$ using Newton-Raphson iteration;

      if *for any* j, $y_{Lj} \geq y_{Lj}^{k-1}$ *and* $y_{Uj} \leq y_{Uj}^{k-1}$ **then**

        flag $\leftarrow$ true

      end

    until *flag = true*;

  until *(*$\|\mathbf{R}_d|_{\mathscr{A}_L \cup \mathscr{A}_U}\| \leq tol_d$ *and* $\|\mathbf{R}_v\| \leq tol_v$*) or* $y_{Lj} > y_{Uj}$ *for some* $j = 1, \ldots, n_d$;

  $k \leftarrow k + 1$;

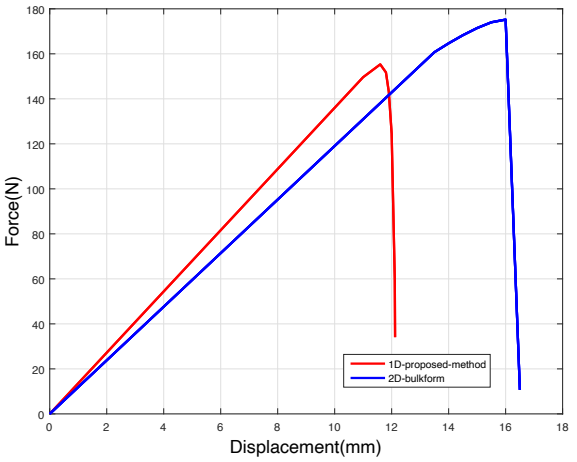

Figure 6: Load-displacement curves from 2D bulk-form phase field method and proposed method.

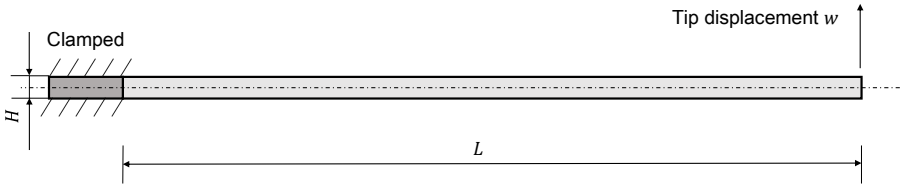

Figure 7: Configuration of a cantilevered beam with transverse displacement load applied at the tip. The beam length is $L = 1000$ mm and the beam height $H = 100$ mm.

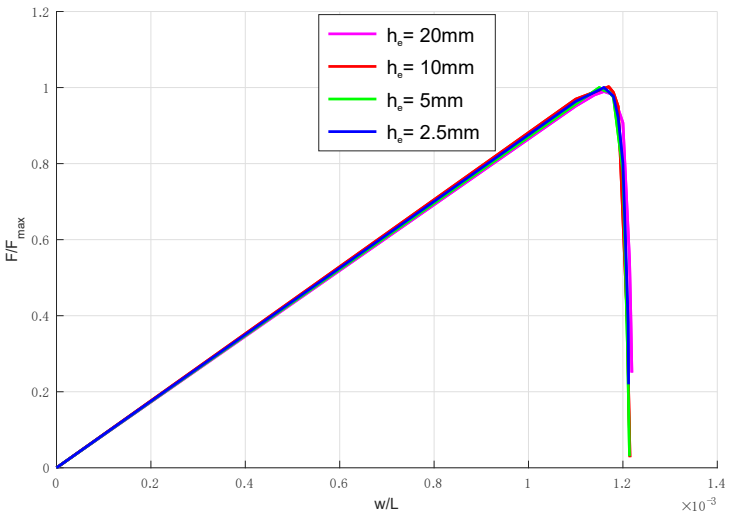

Figure 8: Load-deflection curves for different mesh sizes. Load F is normalized by the maximum load before crack initiation, denoted as $F_{\max}$, and the deflection w is normalized by beam length L.

5.2. A cantilevered beam with two initial cracks at the root

In this example, we consider a cantilevered beam with two initial cracks near the root to verify that cracks in the proposed model behave differently under tension and compression.

The geometric setup as well as the loading are depicted in Figure 11. Located on both sides of the neutral axis, the upper crack is under compression while the lower crack under tension. The beam is loaded up to the collapse of Section A.

The cantilevered beam is subjected to an incrementally increasing displacement load. The displacement field at selected load steps are depicted in Figure 12. Starting from tip displacement $w = 14.0$ mm, a brutal crack growth can be observed by noticing that the graph of the displacement field as a function of x almost becomes a straight line to the right of the cracks. The corresponding phase fields, represented by y_L and y_U, are depicted in Figure 14, where y_L and y_U can roughly be interpreted as crack fronts.

We can only observe gradual propagation of the crack when the tip displacement is small; after a certain load, the crack will brutally propagate. Hence to observe the crack growth process the displacement increments need to be carefully adjusted.

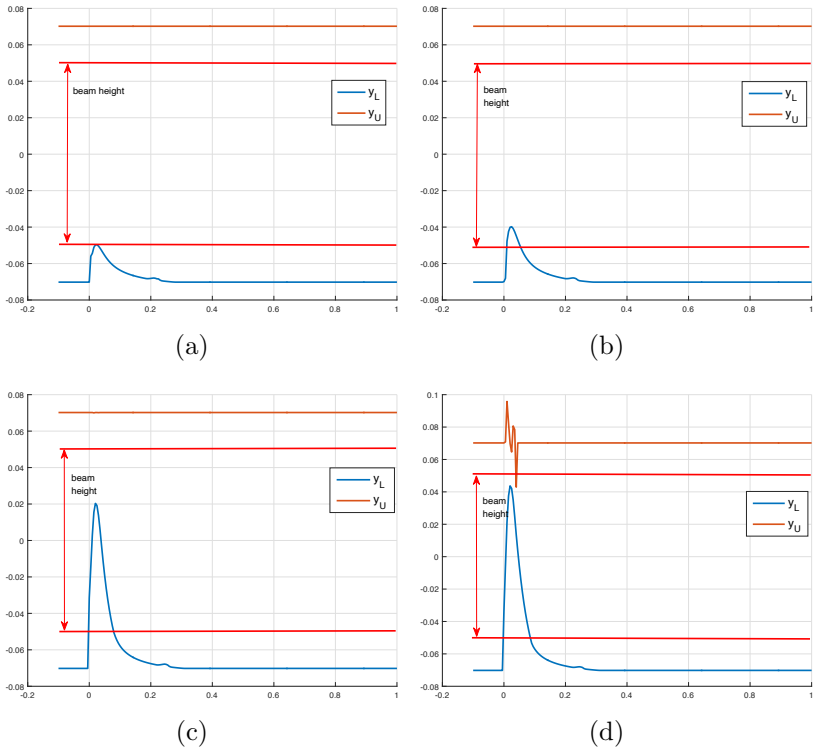

Figure 9: Results of the proposed model for the initially pristine cantilevered beam test: (a) $w = 11.6$ mm; (b) $w = 11.8$ mm; (c) $w = 12.1$ mm, at which the crack length is 0.06 mm; (d) $w = 12.14$ mm, with crack length 0.09 mm.

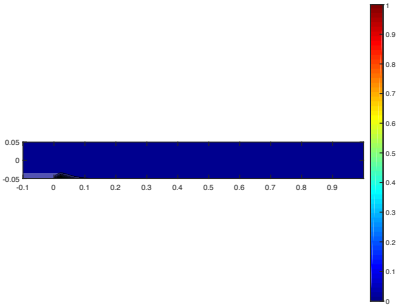
0.05
0
-0.05
-0.1 0 0.1 0.2 0.3 0.4 0.5 0.6 0.7 0.8 0.9
1 0.9 0.8 0.7 0.6 0.5 0.4 0.3 0.2 0.1 0

(a)

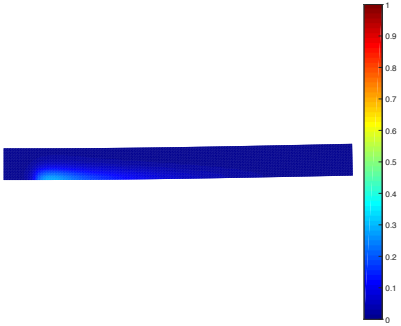
1 0.9 0.8 0.7 0.6 0.5 0.4 0.3 0.2 0.1 0

(b)

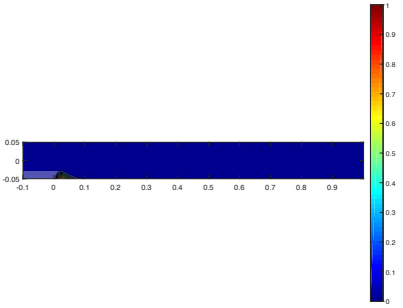
0.05
0
-0.05
-0.1 0 0.1 0.2 0.3 0.4 0.5 0.6 0.7 0.8 0.9
1 0.9 0.8 0.7 0.6 0.5 0.4 0.3 0.2 0.1 0

(c)

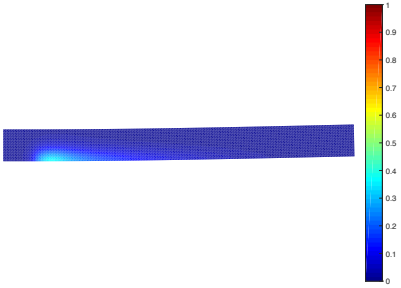
1 0.9 0.8 0.7 0.6 0.5 0.4 0.3 0.2 0.1 0

(d)

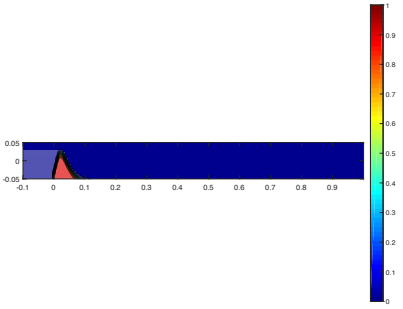
0.05
0
-0.05
-0.1 0 0.1 0.2 0.3 0.4 0.5 0.6 0.7 0.8 0.9
1 0.9 0.8 0.7 0.6 0.5 0.4 0.3 0.2 0.1 0

(e)

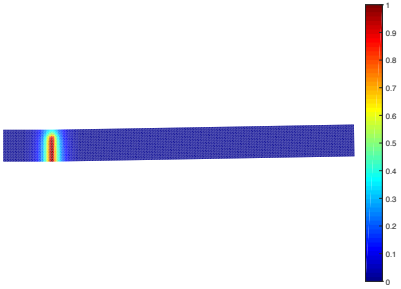
1 0.9 0.8 0.7 0.6 0.5 0.4 0.3 0.2 0.1 0

(f)

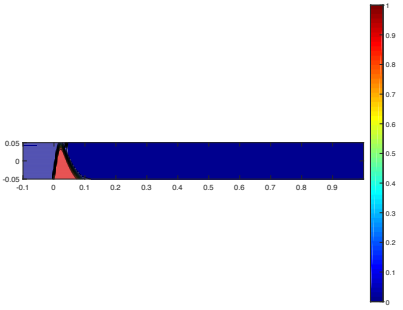
0.05
0
-0.05
-0.1 0 0.1 0.2 0.3 0.4 0.5 0.6 0.7 0.8 0.9
1 0.9 0.8 0.7 0.6 0.5 0.4 0.3 0.2 0.1 0

(g)

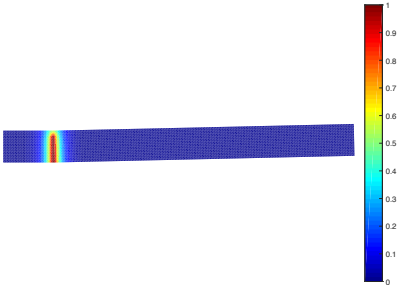
1 0.9 0.8 0.7 0.6 0.5 0.4 0.3 0.2 0.1 0

(h)

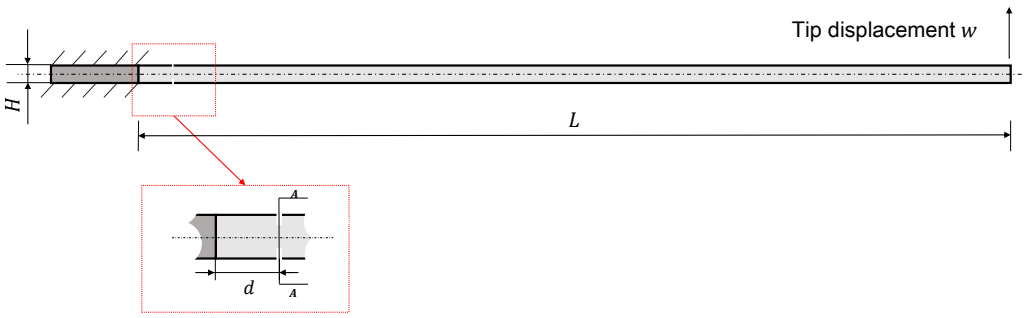

Figure 11: Configuration of a cantilevered beam with two initial cracks, with beam length $L = 1.0$ m, crack distance from the root $d = 0.05$ m, the initial length of the crack is 0.015 m and the beam height $H = 0.1$ m.

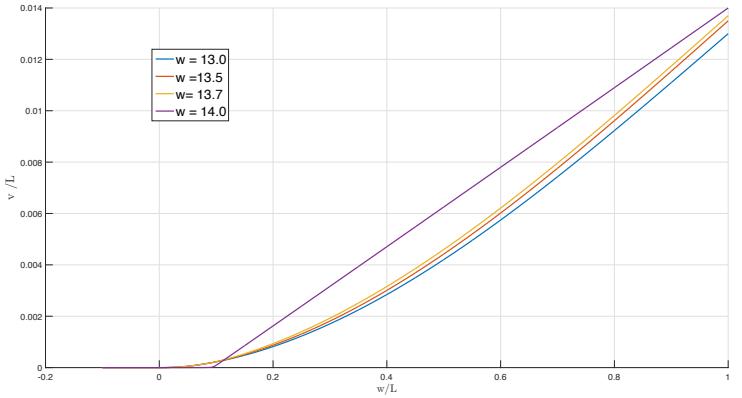

Figure 12: Cantilevered beam with two initial cracks at the root. Displacement field at each load step. Load step 1: tip displacement $w = 13.0$ mm; load step 2: $w = 13.5$ mm; load step 3: $w = 13.7$ mm; load step 4: $w = 14.0$ mm. Length scale parameter ℓ/L=0.02, mesh size h_d/L=h_v/L=0.01, $\beta = 1.0$.

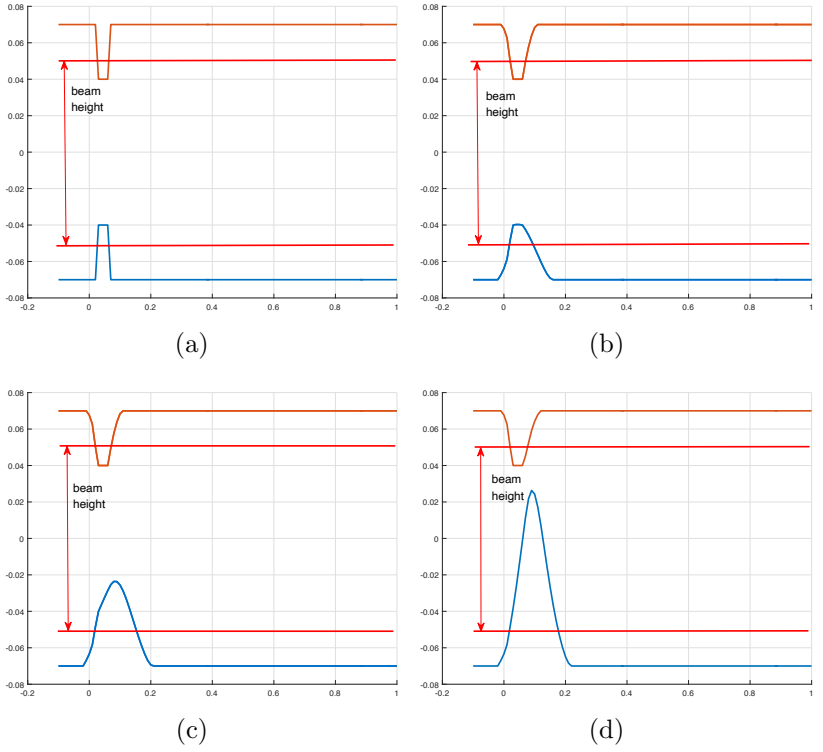

Figure 13: Results of proposed model for cantilevered beam with two initial cracks test: (a) $w = 0$; (b) $w = 13.0$ mm; (c) $w = 13.7$ mm; (d) $w = 14.0$ mm.

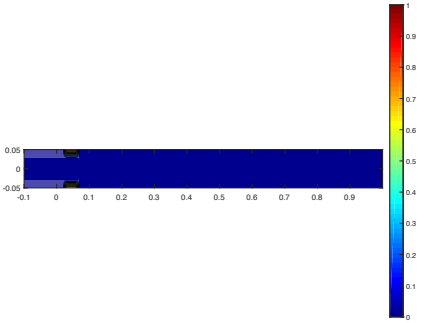
0.05
0
-0.05
-0.1 0 0.1 0.2 0.3 0.4 0.5 0.6 0.7 0.8 0.9
1 0.9 0.8 0.7 0.6 0.5 0.4 0.3 0.2 0.1 0

(a)

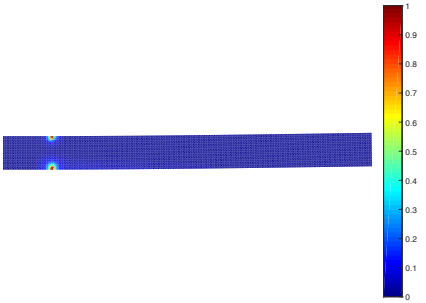
1 0.9 0.8 0.7 0.6 0.5 0.4 0.3 0.2 0.1 0

(b)

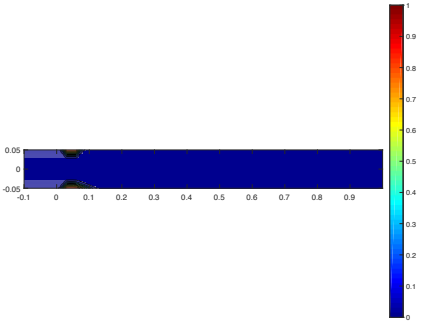
0.05
0
-0.05
-0.1 0 0.1 0.2 0.3 0.4 0.5 0.6 0.7 0.8 0.9
1 0.9 0.8 0.7 0.6 0.5 0.4 0.3 0.2 0.1 0

(c)

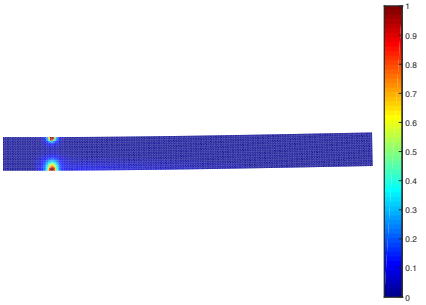
1 0.9 0.8 0.7 0.6 0.5 0.4 0.3 0.2 0.1 0

(d)

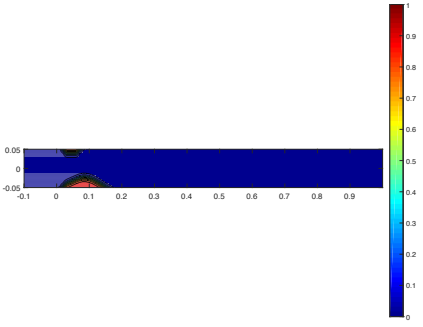
0.05
0
-0.05
-0.1 0 0.1 0.2 0.3 0.4 0.5 0.6 0.7 0.8 0.9
1 0.9 0.8 0.7 0.6 0.5 0.4 0.3 0.2 0.1 0

(e)

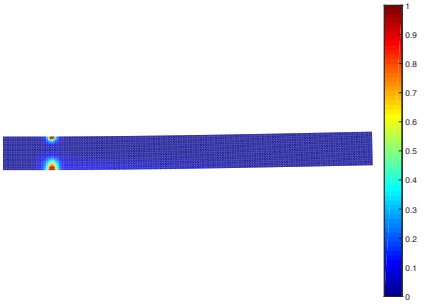
1 0.9 0.8 0.7 0.6 0.5 0.4 0.3 0.2 0.1 0

(f)

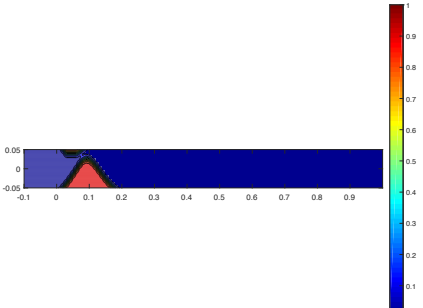
0.05
0
-0.05
-0.1 0 0.1 0.2 0.3 0.4 0.5 0.6 0.7 0.8 0.9
1 0.9 0.8 0.7 0.6 0.5 0.4 0.3 0.2 0.1

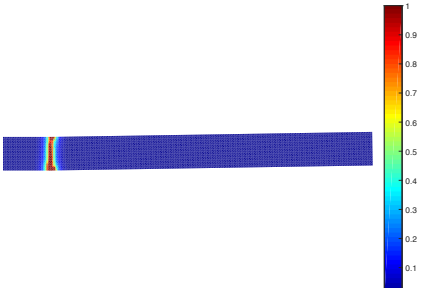
1 0.9 0.8 0.7 0.6 0.5 0.4 0.3 0.2 0.1

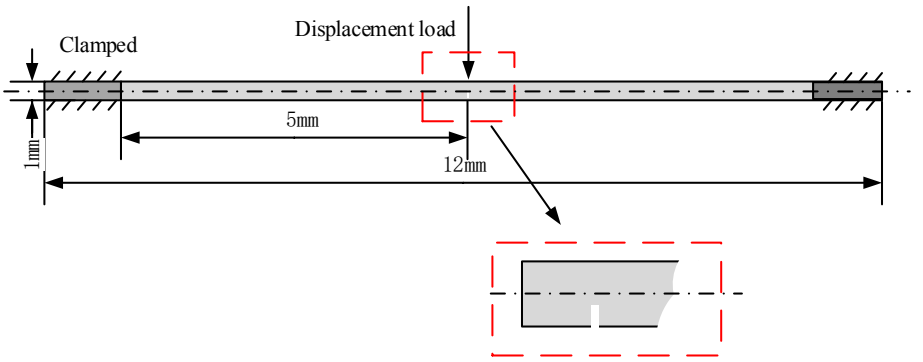

Figure 15: Configuration of a fully clamped beam with one initial crack, under downward displacement loading. The mesh size $h_e = 0.01$ mm, the length parameter $\ell = 0.0125$ mm, and $\beta = 1$.

5.3. A fully clamped beam with one initial crack at the middle

In this numerical example, we set the geometry parameters of fully fixed two ends of the beam, as depicted in Figure 15. We choose the material parameters as follows: $E = 20.8$ kN/mm^2, and $g_c = 5 \times 10^{-4}$kN/mm. The crack propagates as in Figure 16.

In the sequel, we verify the proposed method with the results from Zhang *et al.* [27] with another example of a fully clamped beam with an initial crack, by using the same parameters and boundary conditions, i.e., $E = 268$kN/mm^2, and $g_c = 50$N/m. The comparison is shown in Table 1, indicating that the difference is acceptable.

	proposed method	Zhang *et al.* [27]
Tip displacement (m)	0.04	0.05

Table 1: Comparison with results in the literature using the tip displacement at the same crack length (almost complete fracture).

5.4. A cantilevered curved beam with two initial cracks

In this numerical example, we choose a quarter-circle beam that is fixed at one end and loaded with a transverse tip displacement load at the top end. The problem is depicted in Figure 17. We choose the material parameters as follows: $E = 10^6$ kN/mm^2, and $g_c = 0.4$kN/mm, the height of beam is

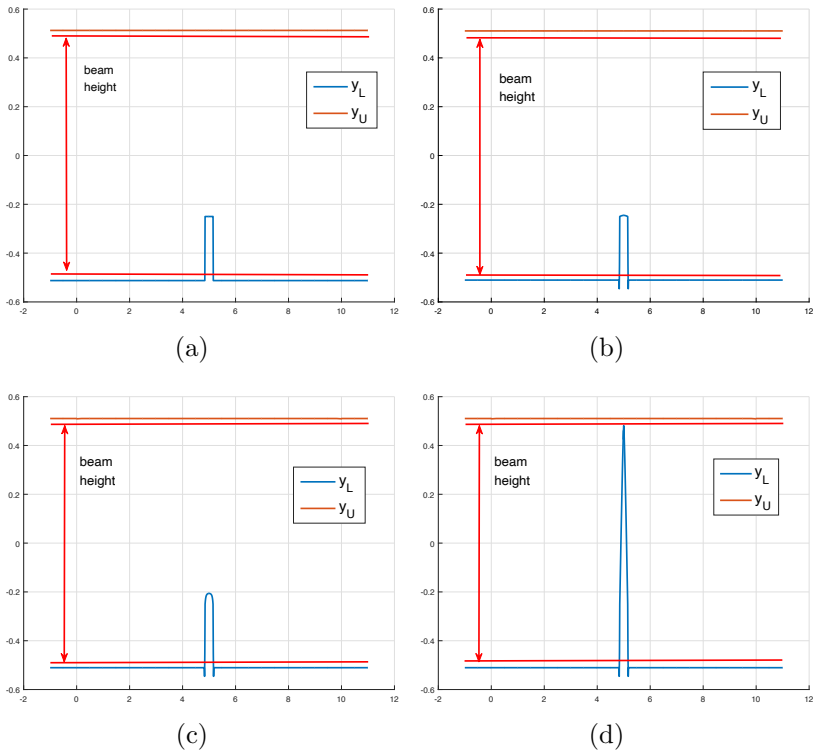

Figure 16: Phase field parameters y_L and y_U for a fully clamped beam with one initial crack at the middle. The tip displacements are: (a) $w = 0$, (b) $w = 0.20$ mm, (c) $w = 0.3262$ mm, (d) $w = 0.32629$ mm.

0.2 m, the radius of the mid-line R is 1 m, $\ell = 0.01$, and $\beta = 2$. The crack propagates as in Figure 18.

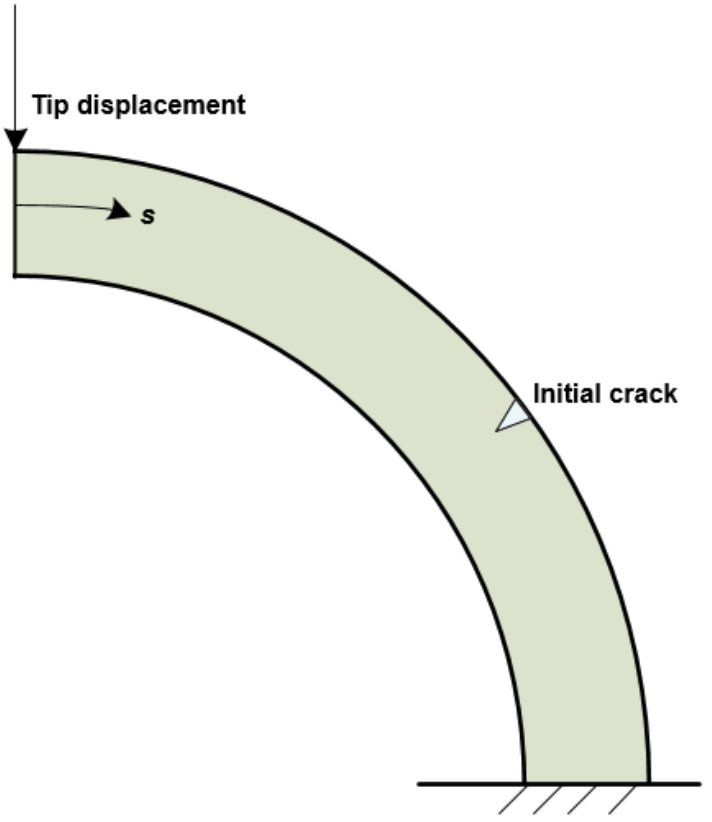

Figure 17: Configuration of a curved-beam with one initial crack.

6. Conclusions

In this paper, we have developed a one-dimensional variational formulation for modeling the brittle fracture in an Euler-Bernoulli beam, which has the ability to handle part-through cracks emanating from the beam edge and orthogonal to the beam axis, typically caused by a bending load. To

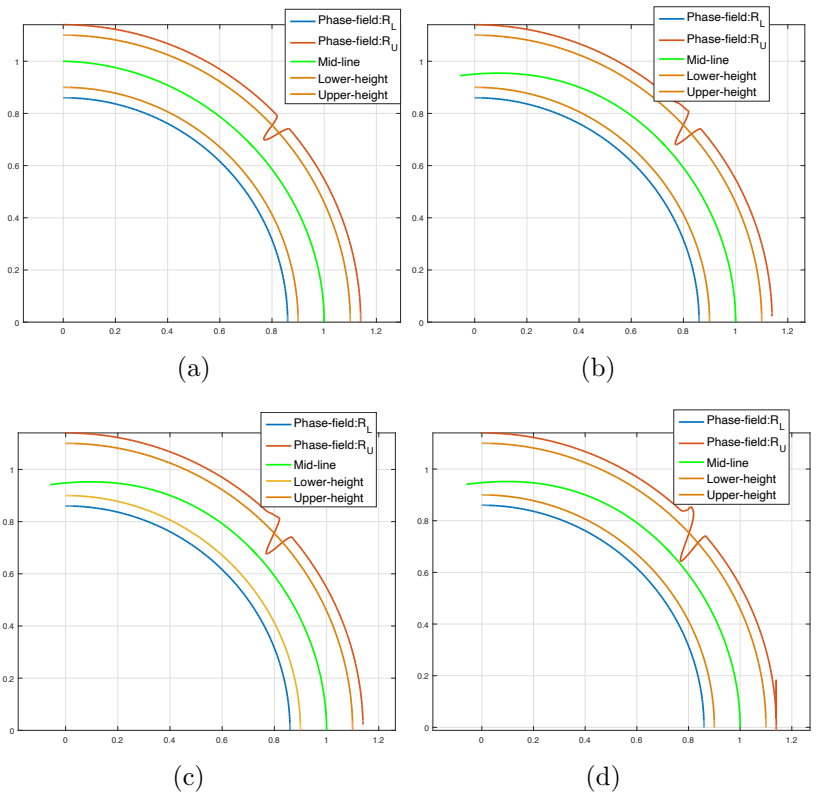

Figure 18: Phase field parameters R_L and R_U (playing the roles of y_L and y_U, respectively) for a curved beam with one initial crack at the upper boundary. The tip displacements are: (a) $w = 0$, (b) $w = 5.5 \times 10^{-2}$, (c) $w = 5.8 \times 10^{-2}$, and (d) $w = 5.9 \times 10^{-2}$.

this end, We introduced a specially designed family of ansätze to the phase field within a cross section. A typical ansatz of the family utilizes two one-dimensional variables to describe the crack extensions. We demonstrated the performance of the proposed beam fracture formulation by means of representative numerical examples with straight and curved beams.

Acknowledgments

This work is supported by the Science Challenge Project, No. TZ2016002.

Appendix A. Useful formulas

A necessary condition for minimization of the total potential energy functional Π_ℓ in (12) is that its first variation vanishes. Thus, we give the expression of the first variation of $\delta\Pi_\ell$.

$$
\begin{aligned}
&\delta\hat{\Pi}_\ell[\overline{v}, y_L, y_U] = \delta\Pi_\ell[\overline{v}, d(y_L, y_U)] \\
&= \frac{1}{2}\int_0^L E\kappa(x)^2\ \delta I(x;\overline{v}, y_L, y_U)\ dx + \int_0^L EI(x;\overline{v}, y_L, y_U)\kappa(x)\delta\overline{v}''(x)\ dx \\
&\quad - M\delta\overline{v}'(x_M) - F\delta\overline{v}(x_F) - \int_0^L w(x)\delta\overline{v}(x)dx \\
&\quad + \int_0^L \int_A g_c\ \delta\gamma[d(x,y;y_L,y_U), \nabla d(x,y;y_L,y_U)]\ dydz\ dx.
\end{aligned}
$$

Here the expression of $\delta\gamma$ can be obtained from (2)

$$
\begin{aligned}
&\delta\gamma[d(x,y;y_L,y_U), \nabla d(x,y;y_L,y_U)] \\
&= \frac{d(x,y;y_L,y_U)\ \delta d(x,y;y_L,y_U)}{\ell} + \ell\delta|\nabla d(x,y;y_L,y_U)|^2.
\end{aligned}
$$

With (9), δd and $\delta|\nabla d|^2$ are given by

$$
\begin{aligned}
\delta d(x,y;y_L,y_U) &= \frac{1}{2}S'[\xi_L(x,y)]\ \delta y_L(x) - \frac{1}{2}S'[\xi_U(x,y)]\ \delta y_U(x) \\
\delta|\nabla d(x,y;y_L,y_U)|^2 &= \frac{2}{\ell^2}\delta\left\{S'[\xi_L(x,y)]\frac{dy_L}{dx} - S'[\xi_U(x,y)]\frac{dy_U}{dx}\right\}^2 \\
&\quad + \frac{2}{\ell^2}\delta\left\{S'[\xi_L(x,y)] - S'[\xi_U(x,y)]\right\}^2,
\end{aligned}
$$

which can be made explicit in terms of $d(\delta y_L)/dx$ and $d(\delta y_U)/dx$ by using

$$\delta S^{(m)}[\xi_L(x,y)] = -\frac{2}{\ell} S^{(m+1)}[\xi_L(x,y)] \frac{d\delta y_L}{dx},$$

and the corresponding formula for y_U, where $S^{(m)}$ denotes the mth derivative of S.

On the other hand, from (11),

$$\delta I(x; \overline{v}, y_L, y_U) = \int_{A(x)} [y - y_{na}(x)]^2 \delta\zeta[d, \kappa(x), y, y_{na}(x)] \, dydz,$$

where $\delta\zeta[d, \kappa, y, y_{na}]$ is given by

$$\delta\zeta[d, \kappa, y, y_{na}] = -2(1-d) H[-(y - y_{na})\kappa] \, \delta d(x, y; y_L, y_U), \quad a.e. \qquad \text{(A.1)}$$

Note that by stating *a.e.* (almost everywhere) in (A.1) we have left out the expressions for the case of $y = y_{na}$, since they will be always multiplying $(y - y_{na})$ in the expressions of δI.

First variation of y_{na}. As stated in Section 3.4, we can either treat y_{na} as dependent on the other fields, and determine it from (10) as needed. Alternatively, we can also treat y_{na} as an independent field. For the latter case, the first variation of $y_{na}(x)$ is given by taking the first variation of (10), which yields

$$\delta y_{na}(x) = \frac{\int_{A(x)} [y - y_{na}(x)] \delta\zeta[d, \kappa(x), y, y_{na}(x)] \, dA}{\int_{A(x)} \zeta[d, \kappa(x), y, y_{na}(x)] \, dA}.$$

References

[1] G. R. Irwin, P. C. Paris, Fundamental aspects of crack growth and fracture, Fracture 3 (1971) 1–46.

[2] H. Okamura, H. W. Liu, C.-S. Chu, H. Liebowitz, A cracked column under compression, Engineering Fracture Mechanics 1 (3) (1969) 547–564.

[3] S. Christides, A. D. S. Barr, One-dimensional theory of cracked Bernoulli-Euler beams, International Journal of Mechanical Sciences 26 (11–12) (1984) 639–648.

[4] A. S. Bouboulas, N. K. Anifantis, Formulation of cracked beam element for analysis of fractured skeletal structures, Engineering Structures 30 (4) (2008) 894–901.

[5] T. Vo-Duy, N. Nguyen-Minh, H. Dang-Trung, A. Tran-Viet, T. Nguyen-Thoi, Damage assessment of laminated composite beam structures using damage locating vector (DLV) method, Frontiers of Structural and Civil Engineering 9 (4) (2015) 457–465.

[6] P. M. A. Areias, T. Belytschko, Non-linear analysis of shells with arbitrary evolving cracks using XFEM, International Journal for Numerical Methods in Engineering 62 (3) (2005) 384–415.

[7] P. M. A. Areias, J. H. Song, T. Belytschko, Analysis of fracture in thin shells by overlapping paired elements, Computer Methods in Applied Mechanics and Engineering 195 (41) (2006) 5343–5360.

[8] B. Bourdin, G. A. Francfort, J.-J. Marigo, Numerical experiments in revisited brittle fracture, Journal of the Mechanics and Physics of Solids 48 (4) (2000) 797–826.

[9] G. A. Francfort, J.-J. Marigo, Revisiting brittle fracture as an energy minimization problem, Journal of the Mechanics and Physics of Solids 46 (8) (1998) 1319–1342.

[10] M. Ambati, T. Gerasimov, L. De Lorenzis, A review on phase-field models of brittle fracture and a new fast hybrid formulation, Computational Mechanics 55 (2) (2015) 383–405.

[11] H. Ulmer, M. Hofacker, C. Miehe, Phase field modeling of fracture in plates and shells, PAMM 12 (1) (2012) 171–172.

[12] F. Amiri, D. Millán, Y. Shen, T. Rabczuk, M. Arroyo, Phase-field modeling of fracture in linear thin shells, Theoretical and Applied Fracture Mechanics 69 (2014) 102–109.

[13] P. Areias, T. Rabczuk, M. A. Msekh, Phase-field analysis of finite-strain plates and shells including element subdivision, Computer Methods in Applied Mechanics and Engineering 312 (2016) 322–350.

[14] M. Ambati, L. De Lorenzis, Phase-field modeling of brittle and ductile fracture in shells with isogeometric NURBS-based solid-shell elements, Computer Methods in Applied Mechanics and Engineering 312 (2016) 351–373.

[15] H. Amor, J.-J. Marigo, C. Maurini, Regularized formulation of the variational brittle fracture with unilateral contact: Numerical experiments, Journal of the Mechanics and Physics of Solids 57 (2009) 1209–1229.

[16] C. Miehe, M. Hofacker, F. Welschinger, A phase field model for rate-independent crack propagation: Robust algorithmic implementation based on operator splits, Computer Methods in Applied Mechanics and Engineering 199 (45–48) (2010) 2765–2778.

[17] J. Kiendl, M. Ambati, L. De Lorenzis, H. Gomez, A. Reali, Phase-field description of brittle fracture in plates and shells, Computer Methods in Applied Mechanics and Engineering 312 (2016) 374–394.

[18] J. Reinoso, M. Paggi, C. Linder, Phase field modeling of brittle fracture for enhanced assumed strain shells at large deformations: formulation and finite element implementation, Computational Mechanics 59 (6) (2017) 981–1001.

[19] C. Miehe, F. Welschinger, M. Hofacker, Thermodynamically consistent phase-field models of fracture: Variational principles and multi-field FE implementations, International Journal for Numerical Methods in Engineering 83 (2010) 1273–1311.

[20] B. Bourdin, G. A. Francfort, J. J. Marigo, The variational approach to fracture, Journal of Elasticity 91 (2008) 5–148.

[21] C. Kuhn, R. Müller, A phase field model for fracture, PAMM 8 (1) (2008) 10223–10224.

[22] C. Kuhn, R. Müller, A continuum phase field model for fracture, Engineering Fracture Mechanics 77 (18) (2010) 3625–3634.

[23] B. S. Gan, An Isogeometric Approach to Beam Structures: Bridging the Classical to Modern Technique, Springer International Publishing, Cham, 2018, pp. 127–156.

[24] M. Dowell, P. Jarratt, The "pegasus" method for computing the root of an equation, BIT Numerical Mathematics 12 (4) (1972) 503–508.

[25] J. Nocedal, S. Wright, Numerical Optimization, Springer-Verlag, New York, 1999.

[26] W. D. Callister, D. G. Rethwisch, Materials Science and Engineering: An Introduction, 7th Edition, Wiley, New York, 2007.

[27] C. Zhang, P. Cao, Y. Cao, J. Li, Using finite element software to simulation fracture behavior of three-point bending beam with initial crack, Journal of Software 8 (5) (2013) 1145–1150.